Petroleum Science 20 (2023) 3841–3853

Contents lists available at ScienceDirect

Petroleum Science

journal homepage: www.keaipublishing.com/en/journals/petroleum-science

Original Paper

Extend ethylene aromatization single-event kinetic modeling with physical and chemical descriptor based on ZSM-5 catalyst

Jia-Rong Xie [a, b, c], Fang Jin [a, b, c, *]

[a] School of Chemical Engineering and Pharmacy, Wuhan Institute of Technology, Wuhan, 430205, Hubei, China
[b] Key Laboratory for Green Chemical Process of Ministry of Education, Wuhan Institute of Technology, Wuhan, 430205, Hubei, China
[c] Novel Reactor & Green Chemical Technology Key Laboratory, Wuhan Institute of Technology, Wuhan, 430205, Hubei, China

ARTICLE INFO

Article history:
Received 3 October 2022
Received in revised form
28 April 2023
Accepted 20 July 2023
Available online 26 July 2023

Edited by Jia-Jia Fei

Keywords:
Kinetic model
Ethylene aromatization
Acid strength distribution
Linear free energy theory

ABSTRACT

The ethylene aromatization is critical for the methanol to aromatics and light alkane dehydroaromatization process. The single-event microkinetic (SEMK) model combining the linear free energy theory and solid acid distribution concept were established and extend for the ethylene aromatization process, which can reduce the kinetic parameters and simplify the reaction network by comparison with the SEMK model including subtype elementary steps based on the type of carbenium ions. Further introducing deactivation parameters φ into the model and applying the linear free energy model to the deactivation experimental data, the obtained deactivation parameters φ indicate that the carbon deposition precursors have the greatest impact on reducing the reaction rate of single-molecular reactions and the smallest impact on the hydrogen transfer reaction. Meanwhile, according to the change of reaction enthalpy, effect of carbenium ion structure on methylation, ethylation, cyclization and endo-β scission was investigated by introducing linear free energy concept into the SEMK model. The effect of different acid strengths on elementary steps was investigated based on the acid strength distribution model, it was found that the methylation and oligomerization reactions, the ali-β scission reaction, endo-β scission reaction and the cyclization reaction were more sensitive to strong acidity sites. The physisorption and chemisorption heat are separated from the protonation heat in the linear free energy kinetic model and the acid strength distribution kinetic model, and the absolute values of the obtained physisorption and chemisorption heat increase with the carbon number of carbenium ions. Furthermore, the parameters of the acid strength distribution kinetic model were applied to propane dehydroaromatization on H-ZSM-5 and the ethane dehydroaromatization on Zn/ZSM-5 to confirm the independence of parameters in the SEMK model with the similar reaction network.

1. Introduction

Light olefins such as ethylene and propylene are important products of petrochemical industry. The sources of light olefins are very wide, coal, diesel, natural gas, biomass and other raw materials can be reacted to obtain light olefin products. Currently, the conventional methods for the production of light olefins are dominated by fluid catalytic cracking (FCC) and steam cracking of naphtha and light diesel oil. In addition, dehydrogenation of alkanes to olefins has also been industrialized, such as dehydrogenation of propane to propylene, and the Oleflex process and Catofin process are currently the main processes (Nawaz, 2015; Zhang et al., 2015). In addition, there are also some processes for producing olefins through small molecule hydrocarbons such as methanol. Methanol to olefins (MTO) is a process in which coal or natural gas is used as raw material to produce olefins. The representative process is the MTO process of UOP/Hydro, the DMTO process of the Dalian institute of chemical physics and the SMTO process of the Sinopec (Li et al., 2020). The obtained light olefins can continue to be used as materials to produce long-chain olefins, aromatics and other gasoline components through chemical processes such as MTG (Methanol to Gasoline), MTA (Methanol to Aromatics) or MOTG (Mobil Olefins to Gasoline and Distillate) (Xu et al., 2021). In addition, aromatics can also be obtained through dehydroaromatization of alkanes like ethane or propane, and this process also includes olefin oligomerization and aromatization. For this type of

* Corresponding author. School of Chemical Engineering and Pharmacy, Wuhan Institute of Technology, Wuhan, Hubei, 430205, China.
E-mail address: fangjin@wit.edu.cn (F. Jin).

https://doi.org/10.1016/j.petsci.2023.07.016

reaction, a bifunctional catalyst is required. Alkanes are dehydrogenated to olefins first, and then olefins participate in oligomerization and aromatization reaction to finally obtain aromatics (Goodarzi et al., 2020; Ma and Zou, 2019; Robinson et al., 2018). In those processes, the oligomerization and aromatization of ethylene are very critical. However, most studies of the oligomerization and aromatization of ethylene are focus on catalyst improvements rather than kinetic studies, because the reaction network from small molecules to larger molecules in this process is too complex. In order to support catalyst design for prediction of product distribution and the industrial scale-up of these processes, the establishment of kinetic model for ethylene oligomerization and aromatization is required.

So far, most of the kinetic studies on hydrocarbon conversion are handled by lumped methods. For the MTG process, Chen and Reagan (1979) used three lumped models (oxygenated hydrocarbons, olefins, aromatics and alkanes), and Chang (1980) established four lumped models (oxygenated hydrocarbons, olefins, methylenes, aromatics and alkanes). Subsequently, Schoenfelder et al. (1994) adopted seven lumped models (oxygenated hydrocarbons, ethylene, propylene, butene, alkanes, methane, carbon dioxide, hydrogen, and water), and Mihail et al. (1983) grouped the reactions of the MTG process into 12 groups, using typical reactants to describe the reaction kinetics. The number of lumps in the kinetic model is increasing, but since the lumped kinetics are not established at the molecular level, the kinetic parameters vary with feedstock composition. This makes it difficult for the established lumped kinetic model to be widely used. Due to the limitations of lumped kinetics, many researchers have turned their attention to building kinetic model at the molecular level.

The SEMK model derived from the detailed reaction network was proposed by Clymans and Froment (1984) and Hillewaert et al. (1988) applied to thermal cracking reactions. They classified complex reaction networks into finite elementary steps and linked the effects of molecular structure and reactivity to kinetic parameters inherent in the reaction, resulting in kinetic parameters that were only related to the type of reaction and type of molecule. Because this method does not require aggregation about the feedstock composition, it is guaranteed that the reaction network is sufficiently detailed. Baltanas et al. (1989) used SEMK theory to study hydrothermal isomerization. Then this method has been introduced to the catalysis process by Vynckier and Froment (1991) for the process with acid catalyst, and the subtype elementary step was introduced to differentiate the activation energy between different carbenium ions in the same elementary steps. Martinis and Froment (2006) applied SEMK theory to the alkylation reaction network of isobutane and butene on proton-exchanged Y-type zeolite by introducing parameters to calculate the heat of protonation of carbenium ions. Pirro et al. (2019) elaborated a methodology based on the SEMK model to kinetics-driven design of heterogeneous catalysts. The kinetically-relevant descriptors were introduced into a combination of fundamental kinetic model to establish descriptor-property relationships between activity and catalyst. Laxmi Narasimhan et al. (2003) studied the transformation process of *n*-octane on Pt-ZSM-22 zeolite, and considered the effect of pore mouths on the reaction. Zhou et al. (2016) investigated the Fischer-Tropsch synthesis with the SEMK model. Moreover, Park and Froment (2001a) established SEMK model of the MTO reaction on ZSM-5 zeolite, and introduced the Evans-Polanyi relationship to analyze the effect of carbon ion type and olefin structure on the rate constant, and deduced the kinetic parameters compared with the subtype elementary steps. They combined SEMK with transition state theory to separate the contribution of the molecular structure to the entropy change of the reaction, resulting in kinetic parameters that are only related to the type of reaction. And since it is only related to the type of reaction, the kinetic model is highly applicable. Alwahabi and Froment (2004) studied the MTO process on SAPO-34 and simulated the deactivation process of the catalyst. Toch et al. (2015) investigated the ethylene oligomerization with the SEMK model according to the initial and terminal steps similar to the polymerization. However, the ethylene aromatization is a process from light hydrocarbon to higher hydrocarbon with a huge reaction network. Based on a new developed reaction network generated by the Bolean relation matrices and vector array method, Jin et al. (2018a) established a kinetic model for the ethylene oligomerization and aromatization process using a SEMK model approach. In addition, most of the ethylene oligomerization and aromatization reactions and the above-mentioned reactions use zeolites as catalyst, and the acid amount, acid type and acid strength of such catalysts are often closely related to the reactivity of the catalyst. And in these processes the kinetic parameters are related to the catalyst with different acidity. Therefore, a kinetic model is tried to establish, which is based on topology of the catalyst with kinetic parameters related with the acidity distribution property of the catalyst.

Many reactions have linear free energy relationships, and the linear free energy relationship is also widely studied in kinetic research. Vojtko and Tomčík (2014) and Wang et al. (2019) derived the Taft equation based on the linear free energy relationship and established a kinetic model for acid-alcohol pairs in the esterification reaction and the hydrogenation reaction of levulinic acid with the Taft equation. The Brønsted equation was used for liquid-phase homogeneous catalytic reaction systems (Brönsted, 1928) to study the relationship between the acid strength of the catalyst and the catalyst performance. Costa et al. (1999) extended the Brönsted-type equation and averaged the acid strength as a benchmark and applied it to solid catalysts. Borges et al. (2005) used the extended Brönsted-type equation to correlate the activation energy of ammonia desorption (DAE), which can be used to describe the acid strength and solid acid-catalyzed *n*-hexane cracking activity. However, the acid strengths on the solid acid surface were not uniform and different acid strengths distributions existed. Subsequently, Jin et al. (2021) and Wang et al. (2020) further correlated the acid strengths distribution with kinetic parameters to study the ethylene oligomerization reaction on MCM-41 and the more complex ethylene oligomerization reaction on ZSM-5 to demonstrate the relationship between acidity and reactivity and to develop a kinetic model, they emphasized the need to analyze the results based on the distribution of different acid strength sites on the solid acid catalyst. In this paper, with the acid distribution concept applied in the solid acid catalysis Brønsted equation, the acid descriptor was introduced into the SEMK model to further study the ethylene oligomerization and aromatization to establish a kinetic model based on the zeolite topology structure for the complex reaction network. And we attempt to incorporate linear free energy theory into SEMK theory and further incorporate acid descriptors into kinetic model to investigate the effect of acid distribution on catalytic performance, thus extending kinetic model whose parameters do not vary with acidity of zeolite catalysts with the same topology to alkane dehydroaromatization.

2. Theory

2.1. Rate equations for the linear free energy kinetic model

According to the single event kinetic theory, by introducing the single-event number (n_e), the influencing factors of reactants and transition state structure on the reaction can be separated from the entropy variation of single-event rate constant. And the rest part of the intrinsic entropy variation was defined as single-event

frequency factor ($\tilde{A}$), the single-event rate constant is defined as Eq. (1). The rate constant of the elementary reaction is defined as Eq. (2).

$$\tilde{k} = \tilde{A}\exp\left(-\frac{E}{RT}\right) \tag{1}$$

$$k' = n_e\tilde{k} \tag{2}$$

The reaction rate of protonation and deprotonation are very fast, so the protonation and deprotonation reaction can be regarded as in a quasi-equilibrium state. The heat of protonation for different carbenium ions needs to be taken into account. The heat of protonation ($\Delta H_{Pr}(O_{ij})$) in the rate equation is divided into seven types according to the carbon number from C_2–C_8. The single-event protonation equilibrium constant can be written as:

$$\tilde{K}_{Pr}(O_{ij}) = \exp\left(\frac{\Delta\tilde{S}_{Pr}}{R}\right)\exp\left(\frac{-\Delta H_{Pr}(O_{ij})}{RT}\right) \tag{3}$$

In addition, in the elementary step with reaction type w, carbenium ion x is converted to another carbenium ion y. O_{ij} stands for the olefin isomer. And the equation for the single-molecule reaction can be written as:

$$r_{w(x:y)} = n_e\tilde{k}_{w(x:y)}\left(\frac{\sigma_{gl}^{O_{ij}}}{\sigma_{gl}^{R_{ik+}}}\right)\tilde{K}_{Pr}(O_{ij})[O_{ij}][H^+] \tag{4}$$

While the equation for the two-molecule reaction can be written as:

$$r_{w(x:y)} = n_e\tilde{k}_{w(x:y)}\left(\frac{\sigma_{gl}^{O_{ij}}}{\sigma_{gl}^{R_{ik+}}}\right)\tilde{K}_{Pr}(O_{ij})[O_{ij}][H^+][M] \tag{5}$$

where, σ_{gl} stands for the global symmetry number.

In light of the Evans-Polanyi relationship, the reaction activation energy changes linearly with the reaction enthalpy ($\Delta H_{w(x:y)}$) of isomers with different carbon numbers, as shown in following Eq. (6).

$$E_{w(x:y)} = E_w^\circ - a_w\left|\Delta H_{w(x:y)}\right| \tag{6}$$

Thus, the single-event rate constant for the elementary step can be written as:

$$\tilde{k}_{w(x:y)} = \tilde{A}_w\exp\left(-\frac{E_w^\circ - a_w\left|\Delta H_{w(x:y)}\right|}{RT}\right) \tag{7}$$

Finally, for the linear free energy model, the reaction rate equation can be derived as follows:

$$r_{w(x:y)} = n_e\left(\frac{\sigma_{gl}^{O_{ij}}}{\sigma_{gl}^{R_{ik+}}}\right)\tilde{A}_w\exp\left(-\frac{E_w^\circ - a_w\left|\Delta H_{w(x:y)}\right|}{RT}\right)\exp\left(\frac{\Delta\tilde{S}_{Pr}}{R}\right)\exp\left(\frac{-\Delta H_{Pr}(O_{ij})}{RT}\right)[O_{ij}][H^+] \tag{8}$$

In our previous research, considering that the type of carbenium ions has a large influence on the activation energy, the SEMK model factors out the effect of molecule and carbenium ion structure of reactant and product on the enthalpy part of reaction rate constant by classifying subtype of elementary step according to energy levels of the reactant and product carbenium ion type. Compared with the previous study (Jin et al., 2021), the introduce of the Evans-Polanyi relationship can further decrease the number of kinetic parameters.

As shown in Table 1, there are 27 parameters in the linear free energy kinetic model. Among them, the intrinsic activation energy (E_w°) and the transfer coefficient (a_w) are inherent properties of the specific reaction which are only determined by the type of reaction.

2.2. Rate equations for the acid strength distribution kinetic model

After establishing the linear free energy model, the acid strength distribution was taken into account as a factor connected to the reaction rate after merging the linear free energy theory with the SEMK model. The ammonia desorption activation energy was used to parametrize the distribution of the acid site. And the concept of acid distribution of solid acid used to apply in the Brønsted equation was introduced to further expand the kinetic model, a new kinetic equation was derived according to the following equations, and another kinetic model was established.

The adsorption of NH_3 as a probe molecule on an acidic catalyst and the reaction of carbenium ions all carried out by protonation. There is a linear relationship between the change in enthalpy of the reaction and the chemisorption heat of NH_3 at the acid sites, and the absolute value of the chemisorption heat of NH_3 and its desorption activation energy is equal (Borges et al., 2005).

$$|\Delta H_r| = a + bE_{Ei} \tag{9}$$

As already mentioned above, the activation energy can be related to the enthalpy change of the reaction.

$$E_w = E_w^\circ - \gamma_p|\Delta H_r| \tag{10}$$

Combining Eqs. (9) and (10), the relationship between reaction enthalpy change and desorption activation energy of the probe molecule (E_{Ei}) can be obtained. The desorption activation energy of the probe molecule was used as the standard of acid strength.

$$E_w = E_w^\circ - \gamma_p a - \gamma_p bE_{Ei} = E_w^\circ - \gamma_w E_{Ei} \tag{11}$$

The expression for the single-event rate constant can be written as:

$$\tilde{k}_w = \tilde{A}_w\exp\left(-\frac{E_w^\circ - \gamma_w E_{Ei}}{RT}\right) \tag{12}$$

Similarly, Eq. (13) can be derived for the protonation reaction and Eq. (14) for the protonation single-event equilibrium constant.

$$\Delta H_{Pr}(O_{ij}) = \Delta H_{Pr}^\circ(O_{ij}) - \gamma_{Pr}E_{Ei} \tag{13}$$

$$\tilde{K}_{Pr}(O_{ij}) = \exp\left(\frac{\Delta\tilde{S}_{Pr}}{R}\right)\exp\left(-\frac{\Delta H_{Pr}^\circ(O_{ij}) - \gamma_{Pr}E_{Ei}}{RT}\right) \tag{14}$$

Substituting Eqs. (12) and (14) into Eq. (4) yields an expression for the reaction rate of the single-molecule reaction at a single acid strength site.

$$r_{Ei,w(x:y)} = n_e\left(\frac{\sigma_{gl}^{O_{ij}}}{\sigma_{gl}^{R_{ik+}}}\right)\tilde{A}_w\exp\left(-\frac{E_w^\circ - \gamma_w E_{Ei}}{RT}\right)\exp\left(\frac{\Delta\tilde{S}_{Pr}}{R}\right)\exp\left(-\frac{\Delta H_{Pr}^\circ(O_{ij}) - \gamma_{Pr}E_{Ei}}{RT}\right)[O_{ij}][H^+]_{Ei} \tag{15}$$

Table 1
Values of the linear free energy kinetic model parameters and the simplified linear free energy kinetic model parameters for ethene oligomerization and aromatization on H-ZSM-5 with Si/Al ratio of 25.

The linear free energy kinetic model		The simplified linear free energy kinetic model		Units
Derived parameter	95% Confidence interval	Derived parameter	95% Confidence interval	
A_{ht}	$3.76 \times 10^{7} \pm 1.01 \times 10^{5}$	A_{ht}	$3.76 \times 10^{7} \pm 1.01 \times 10^{5}$	$s^{-1} \cdot bar^{-1}$
A_{me}	$2.23 \times 10^{8} \pm 1.01 \times 10^{6}$	A_{me}	$2.23 \times 10^{8} \pm 1.01 \times 10^{6}$	$s^{-1} \cdot bar^{-1}$
$A_{ali\text{-}\beta}$	$1.79 \times 10^{9} \pm 1.36 \times 10^{7}$	$A_{ali\text{-}\beta}$	$1.79 \times 10^{9} \pm 1.36 \times 10^{7}$	s^{-1}
A_{cyc}	$3.32 \times 10^{10} \pm 1.03 \times 10^{8}$	A_{cyc}	$3.32 \times 10^{10} \pm 1.03 \times 10^{8}$	s^{-1}
$A_{endo\text{-}\beta}$	$3.19 \times 10^{9} \pm 1.12 \times 10^{7}$	$A_{endo\text{-}\beta}$	$3.19 \times 10^{9} \pm 1.12 \times 10^{7}$	s^{-1}
$A_{exo\text{-}\beta}$	$9.31 \times 10^{1} \pm 1.04 \times 10^{-1}$			s^{-1}
E°_{ht}	$98.86 \pm 8.70 \times 10^{-1}$	E°_{ht}	$97.51 \pm 1.21 \times 10^{-1}$	$kJ \cdot mol^{-1}$
E°_{me}	$92.05 \pm 3.16 \times 10^{-2}$	E°_{me}	$91.88 \pm 3.16 \times 10^{-1}$	$kJ \cdot mol^{-1}$
E°_{di}	$177.02 \pm 4.16 \times 10^{-2}$	E°_{di}	$175.73 \pm 1.17 \times 10^{-1}$	$kJ \cdot mol^{-1}$
$E^{\circ}_{ali\text{-}\beta}$	$146.82 \pm 4.84 \times 10^{-2}$	$E^{\circ}_{ali\text{-}\beta}$	$147.03 \pm 4.84 \times 10^{0}$	$kJ \cdot mol^{-1}$
E°_{cyc}	$155.31 \pm 3.63 \times 10^{-1}$	E°_{cyc}	$157.71 \pm 3.63 \times 10^{-1}$	$kJ \cdot mol^{-1}$
$E^{\circ}_{endo\text{-}\beta}$	$147.69 \pm 4.37 \times 10^{-3}$	$E^{\circ}_{endo\text{-}\beta}$	$148.35 \pm 4.37 \times 10^{-1}$	$kJ \cdot mol^{-1}$
$E^{\circ}_{exo\text{-}\beta}$	$148.52 \pm 2.56 \times 10^{-1}$			$kJ \cdot mol^{-1}$
α_{ht}	$0.0739 \pm 8.20 \times 10^{-4}$	α_{ht}	$0.0703 \pm 1.01 \times 10^{-4}$	
α_{me}	$0.0456 \pm 5.12 \times 10^{-4}$	α_{me}	$0.0429 \pm 5.12 \times 10^{-4}$	
$\alpha_{ali\text{-}\beta}$	$0.3551 \pm 5.05 \times 10^{-4}$	$\alpha_{ali\text{-}\beta}$	$0.3588 \pm 5.05 \times 10^{-4}$	
α_{cyc}	$0.1134 \pm 1.74 \times 10^{-3}$	α_{cyc}	$0.119 \pm 1.74 \times 10^{-3}$	
$\alpha_{endo\text{-}\beta}$	$0.1007 \pm 9.54 \times 10^{-3}$	$\alpha_{endo\text{-}\beta}$	$0.1062 \pm 9.54 \times 10^{-4}$	
$\alpha_{exo\text{-}\beta}$	$0.1025 \pm 6.31 \times 10^{-2}$			
ΔS_{Pr}	$-240 \pm 2.41 \times 10^{0}$	ΔS_{Pr}	$-240 \pm 2.41 \times 10^{0}$	$J \cdot mol^{-1}\ K^{-1}$
$\Delta H_{Pr}(O_2)$	$-58.42 \pm 7.40 \times 10^{-1}$	$\Delta H_{Pr}(O_2)$	$-58.02 \pm 2.27 \times 10^{-1}$	$kJ \cdot mol^{-1}$
$\Delta H_{Pr}(O_3)$	$-92.237 \pm 6.04 \times 10^{-1}$	$\Delta H_{Pr}(O_3)$	$-93.62 \pm 6.04 \times 10^{-1}$	$kJ \cdot mol^{-1}$
$\Delta H_{Pr}(O_4)$	$-101.08 \pm 1.15 \times 10^{-1}$	$\Delta H_{Pr}(O_4)$	$-103.15 \pm 1.14 \times 10^{-1}$	$kJ \cdot mol^{-1}$
$\Delta H_{Pr}(O_5)$	$-117.72 \pm 3.03 \times 10^{-1}$	$\Delta H_{Pr}(O_5)$	$-117.27 \pm 3.02 \times 10^{-1}$	$kJ \cdot mol^{-1}$
$\Delta H_{Pr}(O_6)$	$-126.96 \pm 4.52 \times 10^{-1}$	$\Delta H_{Pr}(O_6)$	$-127.09 \pm 1.76 \times 10^{-1}$	$kJ \cdot mol^{-1}$
$\Delta H_{Pr}(O_7)$	$-138.01 \pm 3.93 \times 10^{-1}$	$\Delta H_{Pr}(O_7)$	$-137.93 \pm 3.93 \times 10^{-1}$	$kJ \cdot mol^{-1}$
$\Delta H_{Pr}(O_8)$	$-142.01 \pm 1.00 \times 10^{-1}$	$\Delta H_{Pr}(O_8)$	$-143.24 \pm 1.00 \times 10^{-1}$	$kJ \cdot mol^{-1}$

The reaction rate is the sum of the rate of all acidic sites on the catalyst, where the acid amount of a single acid strength site (q_{Ei}) corresponding to desorption activation energy (E_{Ei}); γ_w denotes the reaction's sensitivity to the acid strength site of H-ZSM-5 which is divided into five types: methylation/oligomerization reaction, ali-β scission reaction, hydride transfer reaction, cyclization reaction, endo-β scission and protonation reaction.

For different acid strength sites, the total reaction rate is a sum of the rate at each acid strength site.

$$r_{w(x:y)} = \sum_i q_{Ei} r_{Ei,w(x:y)} \tag{16}$$

Therefore, the kinetic model including acid strength distribution can be given as follows:

$$r_w = Lc_{w(x:y)} \tilde{k}_w^{comp} \frac{1}{Da} [O_{ij}] \sum_i \left\{ \exp\left[\frac{(\gamma_w + \gamma_{Pr}) E_{Ei}}{RT} \right] \cdot q_{Ei} \right\} \tag{17}$$

$$(a)\ \tilde{A}_w^{comp} = \tilde{A}_w \exp\left(\frac{\Delta \tilde{S}_{Pr}}{R} \right)$$

$$\tilde{A}_w = \frac{k_B T}{h} \exp\left(\frac{\Delta \tilde{S}^{\circ +}_{int}}{R} \right)$$

$$(b)\ \Delta E_w^{comp} = E_w^{\circ} + \Delta H^{\circ}_{Pr}(O_{ij})$$

$$(c)\ Lc_{w(x:y)} = n_e \left(\frac{\sigma_{gl}^{O_{ij}}}{\sigma_{gl}^{R_{ik^+}}} \right)$$

$$(d)\ \tilde{k}_w^{comp} = \tilde{A}_w^{comp} \exp\left(-\frac{\Delta E_w^{comp}}{R} \right)$$

$$(e)\ D_a = 1 + \sum \{ K_{Pr}(O_{ij}) \cdot [O_{ij}] \}$$

The net formation rate equation of a certain component is obtained by the linear addition of the elementary steps consuming the component and the elementary steps generating the component, which is shown in the supporting information for details. According to the above equation, the number of kinetic parameters to be estimated can be further reduced by the acid strength distribution kinetic model.

2.3. Discrimination of physisorption and chemisorption heat from the protonation heat in the SEMK model

Martinis and Froment (2006), Kumar and Froment (2007), Nguyen et al. (2012) have expounded their own views on the conversion of gas-phase olefins on acidic zeolites. Nguyen et al. proposed the concept of stabilization energies, which represents the energy required for carbenium ions in the gas phase to become carbenium ions at acidic sites, and as shown in Fig. S1 which is energy levels figure for the stabilization energy (Nguyen et al., 2012). According to their concept, the expression for stabilization energy is derived.

$$\Delta E_{stab} = \Delta E_{Chem} - \Delta E_{PA} - \Delta E_{DP} \tag{18}$$

Kumar and Froment also proposed a similar concept, the difference is that they use $\Delta q\,(R^+)$ to represent this similar process. By comparing the states of different energy levels, they are considered to be numerically equivalent (Kumar and Froment, 2007).

$$\Delta E_{stab} = \Delta q(R^+) \tag{19}$$

When estimating the activation energy of elementary steps, Kumar and Froment (2007) proposed the following expression:

$$E_w = E_w^{\circ} + \Delta q(R^+) \tag{20}$$

Combining Eqs. (18)–(20), the following equation can be

derived:

$$E_w = \left(E_w^\circ + \Delta E_{\mathrm{Chem}} - \Delta E_{\mathrm{PA}}\right) - \Delta E_{\mathrm{DP}} = E_w^\circ - \Delta E_{\mathrm{DP}} \tag{21}$$

Because the terms in the brackets are not related to the acidity of the catalyst, the terms are combined and regarded as the intrinsic activation energy E_w°. But ΔE_{DP} is related to the acid strength, which can be associated with the desorption activation energy of ammonia according to the linear free energy theory.

$$|\Delta E_{\mathrm{DP}}| = a + bE_{\mathrm{Ei}} \tag{22}$$

Combining Eqs. (21) and (22), while supplementing the sensitivity coefficient γ to acid strength, the following equation can be derived:

$$E_w = E_w^\circ - \gamma_w E_{\mathrm{Ei}} \tag{23}$$

The resulting Eq. (23) is consistent with Eq. (11), which was used in the acid strength distribution model, but the thinking behind the derivation process is not the same, which shows that the equation of this form is correct and has sufficient physicochemical background.

For the heat of protonation, it is equal to the difference of activation energy between the protonation reaction and the deprotonation reaction. In addition, Kumar and Froment (2007) proposed their expression of heat of protonation:

$$\Delta H_{\mathrm{Pr}} = \Delta E_{\mathrm{Pr}} - \Delta E_{\mathrm{Depr}} = \left[\Delta H_f^g(R^+) - \Delta H_f^g(H^+) - \Delta H_f^g(O)\right] + \Delta q(R^+) \tag{24}$$

Similar to the process of derivation of the activation energy equation, combining Eqs. (18), (19), (22) and (24), the following equation can be derived:

$$\Delta H_{\mathrm{Pr}} = \Delta H_{\mathrm{Pr}}^\circ - \gamma_{\mathrm{Pr}} E_{\mathrm{Ei}} \tag{25}$$

As shown in Fig. S2, the physisorption heat of olefins with the same carbon number is not identical to that of carbenium ions. The physisorption of olefins is necessary for elementary steps, and carbenium ions participate in catalytic elementary step reactions without physical desorption, which leads to the influence of the heat of protonation by the physisorption. Hence, a term representing the heat of physisorption needs to be supplemented in Eq. (26). The terms in the equation, except for the physisorption heat, is considered equal to the chemisorption heat.

$$\Delta H_{\mathrm{Pr}} = \left(\Delta H_{\mathrm{Pr}}^\circ - \gamma_{\mathrm{Pr}} E_{\mathrm{Ei}}\right) + \Delta H_{\mathrm{Phys}} = \Delta H_{\mathrm{Chem}} + \Delta H_{\mathrm{Phys}} \tag{26}$$

2.4. Kinetic experimental data

Both linear free energy model and acid strength distribution model were fitted with experimental data. The experimental data are from the previous literature by Jin et al. (2021) and the experimental data were obtained by three H-ZSM-5 zeolites with different ratios of silicon to aluminum at different temperatures.

When verifying the kinetic parameters, the experimental data of propane aromatization in the literature (Bhan et al., 2005) were used. The experimental data were obtained by reaction on H-ZSM-5, and the rates of production of methane, ethane, ethylene, propene, propane, butane, butene, benzene, toluene, and xylene are reported.

In addition, the ethane dehydroaromatization reaction was carried out in a steel tubular reactor with a diameter of 10 mm. Before the experiment, the Zn/ZSM-5 zeolite was pretreated in the reactor at 873 K under nitrogen for 2 h. After pretreatment, ethane was mixed, and the ratio of ethane and nitrogen was 1:4. The experimental data of different space-times were obtained at 873 K.

The hybrid genetic algorithm including global optimization and local optimization is used to estimate the frequency factors and intrinsic activation energies by directly fitting the experimental results reaction activity instead of two steps through reaction kinetic constant. Fig. 1 shows the optimization process of the objective function with the iteration of the hybrid genetic algorithm with each iteration of a genetic algorithm global optimization and local optimization of Levenberg-Marquardt algorithm.

2.5. Reaction mechanisms

According to the chemical structure of molecules and reaction intermediates, they are classified according to different carbon numbers and reaction types. There are a total of six elementary steps in the reaction network, which are hydride transfer reaction, methylation/oligomerization reaction, ali-β scission reaction, cyclization reaction exo-β scission reaction and endo-β scission reaction. The reaction network contains the components within C_8. The elementary step reactions involved are listed one by one and displayed in Tables S1–S8 in supporting information.

Tables S1 and S2 respectively show all methylation and oligomerization elementary steps involved in the reaction network, methylation refers to C_3–C_6 hydrocarbons react with methyl carbenium ions to increase the length of carbon chain and produce higher carbon number products, while oligomerization is the conversion between ethyl, propyl, butyl carbenium ions and gaseous olefins. Due to the similarity of these two reactions, they are classified as one elementary step in the reflection network. However, the ethylene dimerization reaction is rather special, because the reactants and products of this reaction are primary carbenium ions, and this reaction needs to be considered separately. All ali-β scission reactions are listed in Table S3. As can be seen from Table S4, aromatics and high-carbon cycloalkenes can be generated from linear olefins through the cyclization and hydride transfer or dehydrogenation processes. The cycloolefins and aromatics detected in the experiment are obtained by cyclization. Hydride transfer reaction between carbenium ions and olefins convert the corresponding carbenium ions into hydrocarbons, and

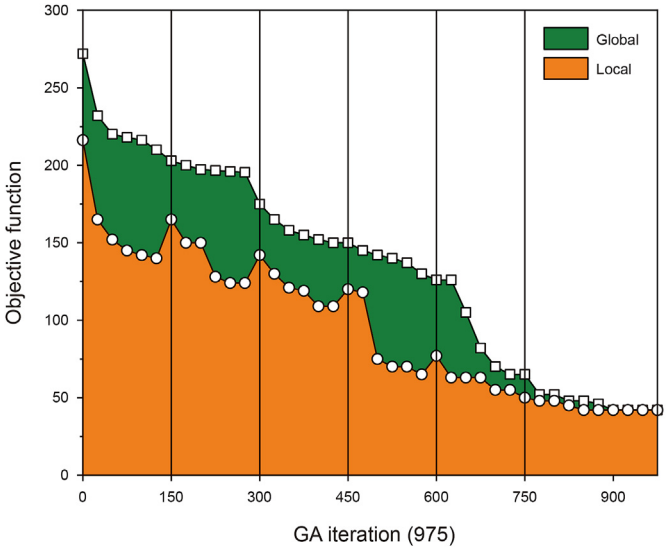

Fig. 1. The optimization process of the objective function with the iteration of the hybrid genetic algorithm. LM, local minimum; GM, global minimum.

ethane and propane are formed in the reaction. And all hydride transfer reactions in the reaction network are listed from Tables S5 and S6. As shown in Tables S7 and S8, corresponding to the formation reaction of cyclic hydrocarbons, the endo-β scission of cyclic hydrocarbons achieves the conversion between cyclic hydrocarbons and straight-chain olefins. And the exo-β scission produces cyclic olefins and chain olefins.

3. Results

3.1. Results of kinetic parameter estimating in linear free energy extend model

As described in 2.1, for the reaction network of ethylene oligomerization and aromatization, the linear relationship between the activation energy of the reaction and the enthalpy change can be obtained by the linear free energy model, so that the reaction rate equation Eq. (6) is obtained. As shown in Fig. 2 at three different temperatures, the experimental yields and the yields calculated by the kinetic model are consistent with each other as the feedstock mass space-time changes. For convenience of observation, the calculated yields are shown in the form of curves. Fig. S3 shows the residuals of the calculated yield values for different temperatures and different mass space-time conditions. Fig. S4 shows a parity plot of experimental yields and corresponding calculated yields for all temperatures, all mass space-time conditions, which are quite similar. The linear free energy kinetic model established contains 27 parameters, and the estimation results of the parameters for the linear free energy model are listed in Table 1.

For the linear free energy kinetic model, the intrinsic activation energy of methylation and oligomerization is 92.05 kJ·mol^{-1}, which is similar to the results (97.496 kJ·mol^{-1}) of Park and Froment (2001b). In particular, for methylation and oligomerization reactions, primary carbon products are not produced in most cases because they are not stable, except for the initial steps that dimerization of ethyl carbenium ions with ethylene. This reaction requires a high activation energy (E°_{di} = 177.02 kJ·mol^{-1}), indicating that this reaction is difficult to occur, but the occurrence of this reaction is an irreplaceable initial elementary step for the entire reaction network. And the intrinsic activation energy of hydride transfer is 98.86 kJ·mol^{-1}, which is similar to the results (91.8 kJ·mol^{-1}) of Martinis and Froment (2006). In addition, the estimated intrinsic ali-β scission activation energy is similar to the result (147.4–162.8 kJ·mol^{-1}) obtained by Standl et al. (2020). For the elementary steps involving aromatic compounds, such as cyclization (E°_{cyc} = 155.31 kJ·mol^{-1}), endo-β scission ($E^{\circ}_{\mathrm{endo}\text{-}\beta}$ = 147.69 kJ·mol^{-1}) and exo-β scission ($E^{\circ}_{\mathrm{exo}\text{-}\beta}$ = 148.52 kJ·mol^{-1}), their intrinsic activation energy is greater than other elementary steps.

The transfer coefficient represents the degree of correlation between the reaction and the enthalpy change of the reaction. It can be seen from Table 1 that the transfer coefficient of the methylation/oligomerization reaction is 0.0456, which means that the effect of the reaction enthalpy change on the methylation/oligomerization reaction activation energy is relatively small, and the transfer coefficient of the methylation/oligomerization reaction is similar to the results of Park and Froment (2001b). The transfer coefficient of hydride transfer reaction (α_{ht} = 0.0739), endo-β scission reaction ($\alpha_{\mathrm{endo}\text{-}\beta}$ = 0.1007) and cyclization (α_{cyc} = 0.1134) is relatively moderate, indicating that the change range of reaction rate constant with reaction enthalpy is not too strong. In addition, ali-β scission reaction ($\alpha_{\mathrm{ali}\text{-}\beta}$ = 0.3551) is more sensitive to the enthalpy change of the reaction, which means that the enthalpy change of this kind of reaction greatly affects reaction rate constant. The heat of protonation of olefins increases with the increase of

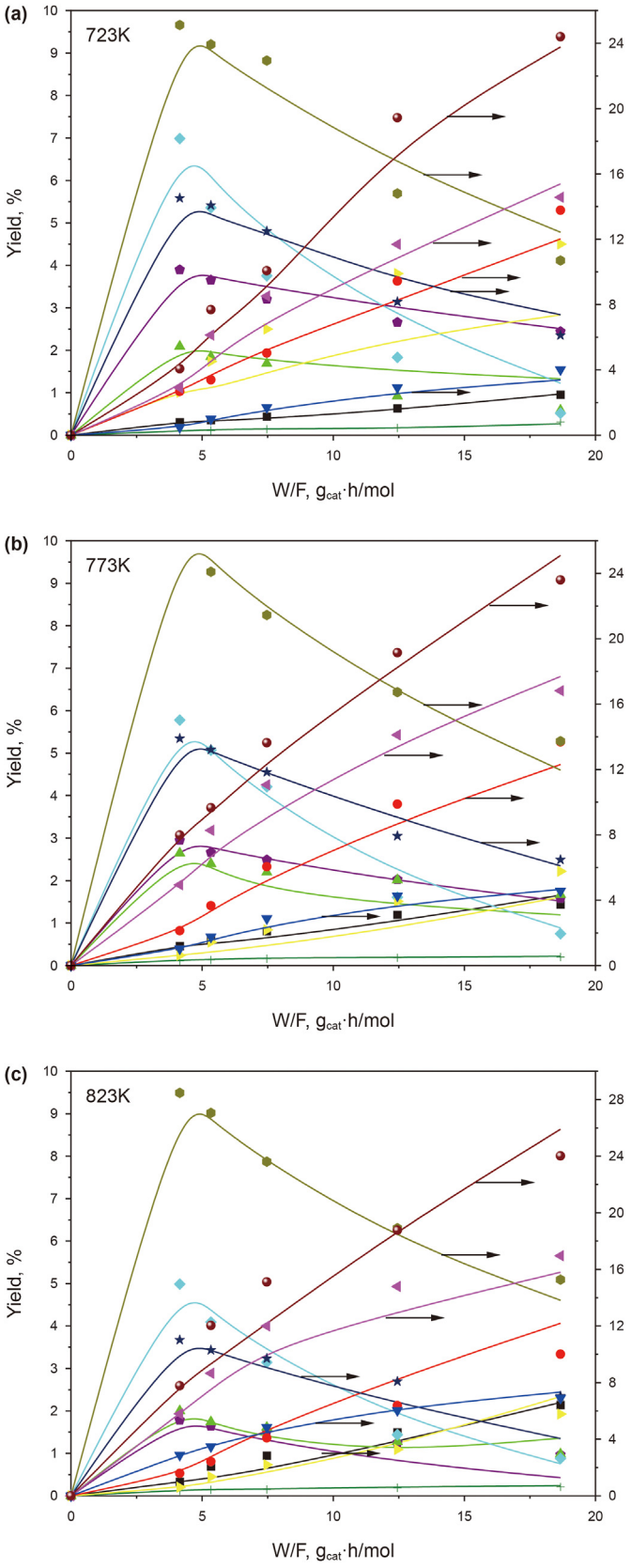

Fig. 2. The effect of space time on product yield at different temperature with the linear free energy model (Si/Al = 25). Methane (+), Ethane (■), Propane (●), Propylene (●), Butene (★), Pentene (▲), Cyclopentene (⬟), Hexene (◆), Heptene (►), Benzene + cyclohexene (▼), Toluene + cycloheptene (◄) and Xylene (◗).

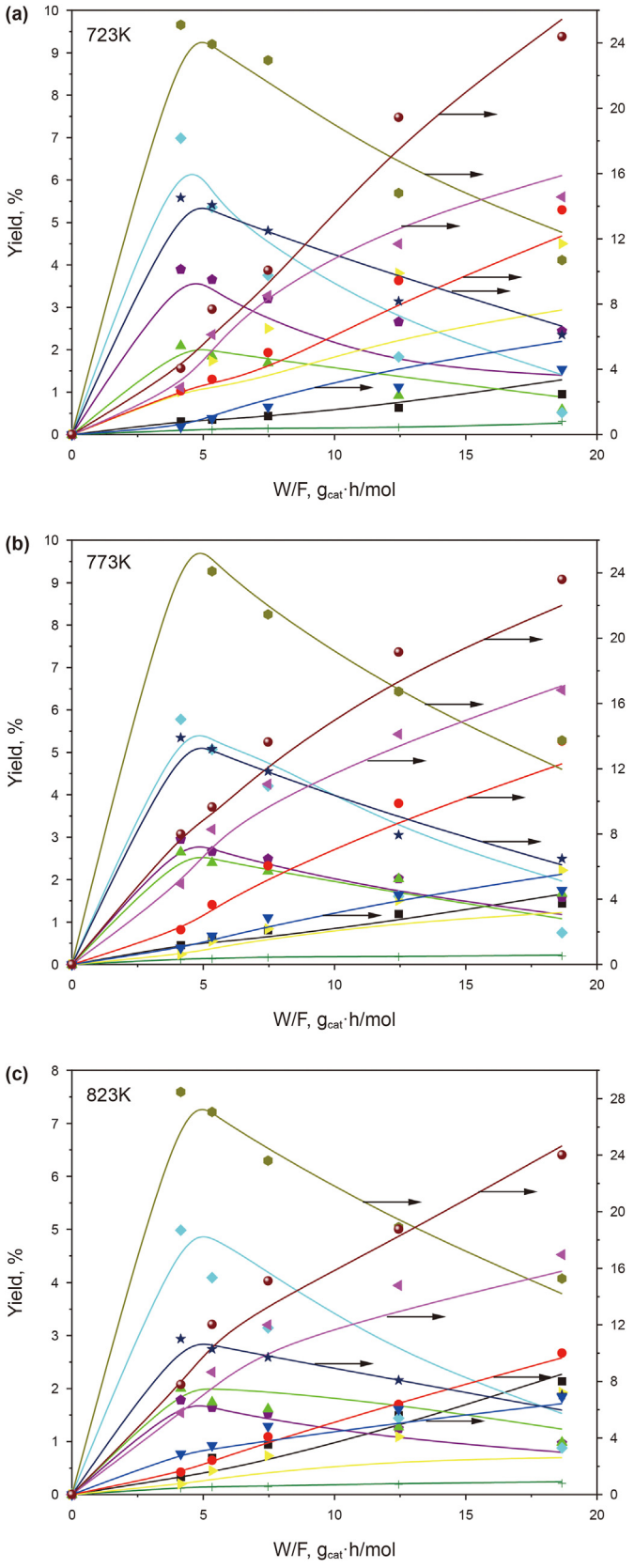

Fig. 3. The effect of space time on product yield at different temperature with the acid strength distribution model (Si/Al = 25). Methane (+), Ethane (■), Propane (●), Propylene (●), Butene (★), Pentene (▲), Cyclopentene (⬟), Hexene (◆), Heptene (▶), Benzene + cyclohexene (▼), Toluene + cycloheptene (◀) and Xylene (◕).

carbon number, which is also in line with carbenium ions chemistry, indicating that the higher the carbon number, the more intense the effect of carbenium ions on the reaction.

3.2. Results of introducing physisorption and chemisorption heat in linear free energy model

For the linear free energy model, it will be further extended by introducing the heat of physisorption and chemisorption in the protonation reaction and adding adsorption-related parameters. According to Eq. (26), the equilibrium constant of protonation in the linear free energy model can be written as Eq. (27). And the reaction rate equation for the single-molecule reaction is shown in Eq. (28).

$$\tilde{K}_{\mathrm{Pr}}(O_{ij}) = \exp\left(\frac{\Delta\tilde{S}_{\mathrm{Pr}}}{\mathrm{R}}\right)\exp\left(-\frac{\Delta H_{\mathrm{Chem}} + \Delta H_{\mathrm{Phys}}}{RT}\right) \tag{27}$$

$$r_{w(x:y)} = n_e \tilde{k}_{w(x:y)}\left(\frac{\sigma_{\mathrm{gl}}^{O_{ij}}}{\sigma_{\mathrm{gl}}^{R_{ik+}}}\right)\exp\left(\frac{\Delta\tilde{S}_{\mathrm{Pr}}}{\mathrm{R}}\right)\exp\left(-\frac{\Delta H_{\mathrm{Chem}} + \Delta H_{\mathrm{Phys}}}{RT}\right)[O_{ij}][H^+] \tag{28}$$

By using the experimental data of ethylene oligomerization and aromatization to fit the parameters in the kinetic model, the values of the parameters of the linear free energy kinetic model in Table 1 except the heat of the protonation reaction were put into the model as fixed values, and only the physisorption and chemisorption heat of the protonation reaction was estimated. The estimated values of physisorption and chemisorption heat of the linear free energy kinetic model are shown in Table 2.

It can be seen from Table 2 that both physisorption and chemisorption heat in protonation reaction vary with the number of carbons of carbenium ions. The chemisorption heat corresponding to C_2 carbenium ions is −39.04 kJ·mol^{-1} and that to C_8 carbenium ions is −78.26 kJ·mol^{-1}, indicating that the smaller the carbon number of carbenium ions emit less chemisorption heat. And the range of the chemisorption heat is also close to those corresponding values reported by Nguyen et al. (2011).

The corresponding physisorption heat of C_2 carbenium ions is −21.69 kJ·mol^{-1} and that of C_8 carbenium ions is −66.24 kJ·mol^{-1}, indicating that the heat of physisorption also has a similar phenomenon that the smaller the carbon number of carbenium ions will emit less physisorption heat during the reaction.

3.3. Extended application of linear free energy model to deactivation experimental data

The SEMK model can be extended by adding kinetic parameters. In the experiment, it was found that for the H−-ZSM−-5 catalyst with Si/Al molar ratio of 25, under determined temperature and space time, the catalyst activity decreased with reaction time due to catalyst deactivation.

It is known that the deactivation of H−-ZSM−-5 is mainly due to the production of carbon deposition precursors. As the reaction time increases, the carbon deposition precursors cover the acidic sites on the catalyst, and due to its size and structure, it cannot be desorbed from the catalyst, resulting in a decrease in catalyst activity. At the same time, carbon deposition precursors also occupy pore space, hindering the diffusion of macromolecular products from the pores and hindering the progress of the reaction. In the study of deactivation kinetics for catalytic cracking, the C_9^+component is generally believed to irreversibly adsorb on the

Table 2
Value of adsorption-related parameters of the linear free energy model and the simplified linear free energy kinetic model.

Derived parameter	The linear free energy kinetic model	The simplified linear free energy kinetic model	Units
	95% Confidence interval	95% Confidence interval	
ΔH_{Chem} (O_2)	$-39.04 \pm 6.24 \times 10^{-1}$	$-39.61 \pm 2.41 \times 10^{-1}$	kJ·mol^{-1}
ΔH_{Chem} (O_3)	$-48.7 \pm 5.98 \times 10^{-1}$	$-50.17 \pm 7.52 \times 10^{-1}$	kJ·mol^{-1}
ΔH_{Chem} (O_4)	$-55.02 \pm 6.77 \times 10^{-1}$	$-52.94 \pm 4.83 \times 10^{-1}$	kJ·mol^{-1}
ΔH_{Chem} (O_5)	$-58.19 \pm 2.05 \times 10^{-1}$	$-59.5 \pm 4.58 \times 10^{-1}$	kJ·mol^{-1}
ΔH_{Chem} (O_6)	$-67.63 \pm 5.37 \times 10^{-1}$	$-64.52 \pm 8.47 \times 10^{-1}$	kJ·mol^{-1}
ΔH_{Chem} (O_7)	$-74.55 \pm 2.76 \times 10^{-1}$	$-73.29 \pm 6.31 \times 10^{-1}$	kJ·mol^{-1}
ΔH_{Chem} (O_8)	$-78.26 \pm 4.28 \times 10^{-1}$	$-78.38 \pm 7.55 \times 10^{-1}$	kJ·mol^{-1}
ΔH_{Phys} (O_2)	$-21.69 \pm 5.26 \times 10^{-1}$	$-20.87 \pm 2.62 \times 10^{-1}$	kJ·mol^{-1}
ΔH_{Phys} (O_3)	$-43.31 \pm 8.33 \times 10^{-1}$	$-42.04 \pm 4.09 \times 10^{-1}$	kJ·mol^{-1}
ΔH_{Phys} (O_4)	$-47.85 \pm 2.41 \times 10^{-1}$	$-49.75 \pm 8.28 \times 10^{-1}$	kJ·mol^{-1}
ΔH_{Phys} (O_5)	$-54.85 \pm 3.62 \times 10^{-1}$	$-56.96 \pm 5.44 \times 10^{-1}$	kJ·mol^{-1}
ΔH_{Phys} (O_6)	$-59.86 \pm 5.24 \times 10^{-1}$	$-60.13 \pm 6.18 \times 10^{-1}$	kJ·mol^{-1}
ΔH_{Phys} (O_7)	$-63.24 \pm 7.41 \times 10^{-1}$	$-64.27 \pm 2.51 \times 10^{-1}$	kJ·mol^{-1}
ΔH_{Phys} (O_8)	$-66.24 \pm 3.97 \times 10^{-1}$	$-67.27 \pm 1.82 \times 10^{-1}$	kJ·mol^{-1}

surface of acidic catalysts and act as deposition carbon precursors to cover the acidic sites on the catalyst, leading to catalyst deactivation (Martinis and Froment, 2006). The catalyst selected for the experimental data of the deactivation mechanics model is H-ZSM-5 zeolite with Si/Al molar ratio of 25. Experimental data obtained after continuous reaction for 7 h under the conditions of reaction temperature of 723 K, reaction pressure of atmospheric pressure, and reaction space time of 7.47, 12.4, and 18.7 $g_{cat}\cdot h\cdot mol^{-1}$, respectively.

An empirical kinetic equation for deactivation has been proposed as shown in Eq. (29) to explain the deactivation effect of carbon deposition precursors on the reaction by introducing the deactivation equation with β and C_c in the rate of elementary steps, where β is a constant and C_c stands for the content of carbon deposition precursor (Moustafa and Froment, 2003).

$$\varphi = \exp(-\beta C_c) \tag{29}$$

Since β and C_c are unknowns in the equation, the value of the whole equation φ is taken as the kinetic parameter in the kinetic model. In the reaction, due to the formation of carbon deposition precursors various types of elementary steps undergo varying degrees of deactivation. Therefore, in the kinetic model, only one deactivation equation value is used for all elementary steps, which is not enough. Referring to the literature of Moustafa and Froment (2003), a total of three values of deactivation equations were introduced in the model, each corresponding to one or several types of elementary steps. The corresponding relationship between the values of deactivation equations and elementary steps is shown in Table S12.

The first deactivation parameter, φ_1, is assigned to an elementary step that can be considered a two-molecular reaction, hydrogen transfer reaction, where the reactants involve molecules and carbenium ions. The second deactivation parameter, φ_2, is associated with the alkylation reaction, which is also a two-molecular reaction. The third deactivation parameter, φ_3, is associated with the elementary steps belonging to single-molecular reaction, such as cyclization reaction, ali-β scission reaction, and endo-β scission reaction. Referring to Froment's point of view (Froment, 1991, 1997), the effect of carbon deposition precursors on the elementary steps is explained by multiplying the value of deactivation function in the rate equation, and the rate equation of the reaction will be written as Eqs. (30) and (31).

$$r_{w(x:y)} = k_{w(x:y)}\left[R_{ik}^{+}\right]\varphi_i \tag{30}$$

$$r_{w(x:y)} = k_{w(x:y)}\left[R_{ik}^{+}\right][M]\varphi_i \tag{31}$$

The values of other kinetic parameters contain of the linear free energy model in Tables 1 and 2, including heat of physisorption and heat of chemisorption, were fixed, and the newly introduced deactivation parameter φ was estimated using the deactivation experiment data. The estimated results are shown in Table 3 where the value of φ_1 is 0.9769, indicating that the reaction rate of hydrogen transfer reaction is least affected by coke compared with other reaction types. The values of φ_2 and φ_3 are 0.8721 and 0.8653 respectively, indicating that the carbon deposition precursors have less influence on the reaction rate of two-molecular reactions such as alkylation. The cyclization and other single-molecular reactions are more affected by carbon deposition precursors and the reaction rate decreases more.

The fitting results of the deactivated kinetic model are shown in Fig. S5. The points in the figure are the component yields measured by experiment, and the curve is the yields calculated by the kinetic model at the corresponding space time. It can be seen that the kinetic model fits the experiment data well. The results show that the model can predict the spatial and temporal trends of the components in the case of catalyst deactivation. Figs. S6 and S7 are the residual diagram and parity plot of experimental values and calculated values respectively, indicating that it is feasible to extend the linear free energy kinetic model to the deactivated data.

3.4. Results of kinetic parameter estimating in acid strength distribution extend model

After the linear free energy model is established, the effect of the catalyst acid strength distribution on the reaction activity will be further considered to decrease the number of kinetic parameters. Eq. (15) shows a rate equation after introducing the acidity descriptor. By associating different types of elemental steps with the acid strength distribution of zeolite with sensitivity factor (γ), the relationship between them can be analyzed quantitatively. Due to the kinetic model is related to the acid strength of the catalyst, the experimental data on H-ZSM-5 with different silicon aluminum ratio are considered. Fig. 3, Figs. S10 and S13 show the yield obtained by the model of the acid strength distribution model and the

Table 3
The values of deactivation parameters in the linear free energy model deactivation kinetic model.

Derived parameter	95% Confidence interval
φ_1	$0.9769 \pm 4.27 \times 10^{-3}$
φ_2	$0.8721 \pm 2.74 \times 10^{-3}$
φ_3	$0.8653 \pm 7.38 \times 10^{-3}$

experimental yield on H-ZSM-5 with Si/Al = 25, 60, 70 respectively, and those also show a high agreement. Figs. S8, S11 and S14 are diagrams of the residuals between the experimental yield and the calculated yield, which also illustrates the reliability of the model. Figs. S9, S12 and S15 are parity plots between the experimental yield and the calculated yield. The acid strength distribution model includes 19 kinetic parameters, and the estimation results of the parameters are listed in Table 4.

Comparing the intrinsic activation energies of Tables 1 and 4, it can be seen that the most intrinsic activation energy of the acid strength distribution model is larger than that of the linear free energy model, which does not indicate the reaction activation energy of elementary steps has obvious change with those of linear free energy kinetic model. The reaction activation energy of the acid strength distribution model is stripped of intrinsic activation energy from the contribution of acid sites to the activation energy. For the acid strength distribution model, its main feature is to separate the sensitivity factor of different reaction types to acid strength. For methylation and oligomerization reactions, the sensitivity factor of them is 0.05444, indicating that these reactions are sensitive to acid strength. For hydride transfer reactions, the products of this reaction are alkanes, it can be seen from Table 4 that its sensitivity factor is 0.02143, which means that this kind of reaction is not sensitive to strong acid sites. Table 4 shows that the sensitivity factors of the cyclization reaction and the endo-β scission reaction ($\gamma_{cyc} = 0.04164$, $\gamma_{endo\text{-}\beta} = 0.05275$), which illustrates the situation that these two types of reactions require higher acid strength sites, indicating that more strong acid sites can obviously increase the activity of these two types of reactions. This is also confirmed by the experimental results that with the increase of acidity strength, the aromatics selectivity is increased. The sensitivity factor 0.07513 of ali-β scission reaction is highest in these elementary steps, indicating that higher acid strength sites can promote the reaction to a greater extent. And the sensitivity factor of the protonation heat is 0.02963, which is relatively low. It can be deduced that olefins protonation can be performed with the weak acid sites (Derouane et al., 2013).

3.5. Results of introducing physisorption and chemisorption heat in acid strength distribution model

In order to introduce adsorption-related parameters into the acid strength distribution model, the equation of protonation equilibrium constant is extended according to Eq. (26). The rate equation of the single-molecule reaction at a single acid strength site is shown in Eq. (32).

$$r_{Ei,w_{(x:y)}} = n_e \left(\frac{\sigma_{gl}^{O_{ij}}}{\sigma_{gl}^{R_{ik+}}}\right) \tilde{A}_w \exp\left(-\frac{E_w^{\circ} - \gamma_w E_{Ei}}{RT}\right) \exp\left(\frac{\Delta\tilde{S}_{Pr}}{R}\right) \exp\left(-\frac{\Delta H_{Chem}^{\circ} + \Delta H_{Phys}^{\circ}}{RT}\right) [O_{ij}][H^+]_{Ei} \quad (32)$$

The values of kinetic parameters except heat of protonation in Table 4 were used as fixed values to estimate the values of intrinsic chemisorption heat and intrinsic chemisorption heat. And the results obtained are shown in Table S13 value of intrinsic physisorption heat was −58.26 kJ·mol^{-1}, and value of intrinsic chemisorption heat was −64.37 kJ·mol^{-1}.

Table 4
Values of the acid strength distribution kinetic model parameters for ethene oligomerization and aromatization on H-ZSM-5 with Si/Al ratio of 25, 60 and 70.

Derived parameter	95% Confidence interval	Values
A_{ht}	$3.76 \times 10^7 \pm 1.01 \times 10^5$	s^{-1}·bar^{-1}
A_{me}	$2.23 \times 10^8 \pm 1.01 \times 10^6$	s^{-1}·bar^{-1}
$A_{ali\text{-}\beta}$	$1.79 \times 10^9 \pm 1.36 \times 10^7$	s^{-1}
A_{cyc}	$3.32 \times 10^{10} \pm 1.03 \times 10^8$	s^{-1}
$A_{endo\text{-}\beta}$	$3.19 \times 10^9 \pm 1.12 \times 10^7$	s^{-1}
E°_{ht}	$95.48 \pm 4.10 \times 10^{-1}$	kJ·mol^{-1}
E°_{me}	$93.17 \pm 3.12 \times 10^{-2}$	kJ·mol^{-1}
E°_{di}	$181.91 \pm 5.45 \times 10^{-2}$	kJ·mol^{-1}
$E^{\circ}_{ali\text{-}\beta}$	$148.34 \pm 7.24 \times 10^{-2}$	kJ·mol^{-1}
E°_{cyc}	$161.21 \pm 7.35 \times 10^{-1}$	kJ·mol^{-1}
$E^{\circ}_{endo-\beta}$	$150.75 \pm 5.83 \times 10^{-1}$	kJ·mol^{-1}
γ_{ht}	$0.02143 \pm 2.28 \times 10^{-4}$	
γ_{me}	$0.05444 \pm 5.45 \times 10^{-4}$	
$\gamma_{ali\text{-}\beta}$	$0.07513 \pm 8.74 \times 10^{-4}$	
γ_{cyc}	$0.04164 \pm 5.21 \times 10^{-4}$	
$\gamma_{endo\text{-}\beta}$	$0.05275 \pm 4.32 \times 10^{-4}$	
γ_{Pr}	$0.02963 \pm 7.53 \times 10^{-4}$	
ΔS_{Pr}	$-248.45 \pm 4.70 \times 10^0$	J·mol^{-1}·K^{-1}
ΔH_{Pr}	$-119.36 \pm 6.81 \times 10^0$	kJ·mol^{-1}

4. Discussion

4.1. Intruding of linear free energy and acid strength concept in kinetic model to reduce the number of kinetic parameters and simplify reaction network

The introduction of Evans-Polanyi linear free energy concept can reduce the single-event kinetic parameters by comparing with our previous work of introducing the subtype elementary steps according to the carbenium ion types in elementary steps. As shown in Tables 1 and it can be seen that based on the linear free energy concept each elementary step only have one intrinsic activation energy (E_w°) and the transfer coefficient (a_w) without discrimination of carbenium ions type of reactant and products. Moreover, with comparison single-event kinetic parameters of acid strength distribution model with the previous kinetic model (Jin et al., 2021), the numbers of parameters were further reduced from 27 to 19. Although the acid strength distribution model has fewer kinetic parameters, it can fit the experimental data as well as that of the previous kinetic model.

Moreover, because the SEMK model is established based on the detailed reaction network generated by the computer algorithm, the reaction network can be shrink by elimination of some insignificant elementary steps according to the rate constants value calculated by kinetic parameters, which can further reduced the kinetic parameters. According to the single-event kinetic parameters of the Evans-Polanyi linear free energy concept incorporated kinetic model in Table 1, the reaction rate constants were calculated and listed in Table S9. It is worth noting that the rate constants for exo-β scission reactions are exceptionally smaller than other elementary steps. The exo-β scission reactions are mainly proceeded through the side chain of cyclic hydrocarbon to generate light alkanes or olefins. Considering almost no C_8^+ hydrocarbon was observed in this work, the lower possibility for this elementary step. Therefore, this elementary step can be omitted from the reactive network. As shown in Table 1, the values of kinetic parameters in the simplified linear free energy kinetic model are basically the same with kinetic parameters unreduced linear free energy kinetic model. Moreover, the rate constants of the simplified linear free energy kinetic model are listed in Table S10. The single-event kinetic parameters of the acid strength distribution model in Table 4 are calculate to compare the single-event rate constant on H-ZSM-5 (Si/Al = 25) for reaction network simplification, and the results can be found in Table S11.

By comparison of the elementary step reaction rate constant based on acid strength distribution concept with those corresponding values based on the previous kinetic parameters of

subtype elementary steps in reference (Jin et al., 2021), the value of $k_{ht(s:t)}$, $k_{alkyl(s:t)}$, $k_{cyclic(s:s)}$, $k_{ali\text{-}\beta(s:p)}$ and $k_{ali\text{-}\beta(t:s)}$ in Table 6 of reference (Jin et al., 2021) for the subtype elementary steps is much smaller than that corresponding elementary steps of the acid strength distribution kinetic model in Table S11. It can be considered that these five subtype elementary steps have less influence on the reaction network compared with other subtype elementary steps, which can be simplified in the reaction network by the magnitude difference of the single-event rate constants. Table S11 shows the single-event rate constants of kinetic model containing subtype elementary steps in the simplified subtype reaction network and those of the acid strength distribution model, it can be found that the rate constants of remaining subtype elementary steps are close to the corresponding rate constants of the acid strength distribution model, which confirmed the reaction network simplify can be performed by the kinetic model.

After calculating the single-event rate constant, the several elementary reactions were selected as examples to confirm the relative value of rate constant of different elementary steps in those models are closed. The reaction rate of the linear free energy model which is calculated based on Eq. (6) and the reaction rate of the acid strength distribution model which is calculated based on Eq. (15), are listed in Table 5. The rate calculated from three kinetic models were compared with the data of ethylene aromatization on H-ZSM-5 (Si/Al = 25) at 823 K and space-time 5.33 $g_{cat}\cdot h\cdot mol^{-1}$. As can be seen from Table 5, the values corresponding to a certain reaction with three kinetic model are within the same range, and the difference is no more than one order of magnitude, indicating that the results obtained are reliable.

4.2. Influence of carbenium ion structure on the elementary steps rate coefficients based on the linear free energy model

For the linear free energy model, the rate constant of the reaction is related to the enthalpy change of the reaction. Fig. 4(a) shows the effect of the chain length of the reactants on the reaction rate constant of the methylation/oligomerization, cyclization and endo-β scission at 723 K. In the methylation/oligomerization steps of linear olefins included in the reaction network, the rate constant increases with the increase of the carbon number of the reactant. This result is consistent with the calculated results of Park and Froment (2004). According to Eq. (5), the frequency factor, the intrinsic activation energy and the transfer coefficient for a single reaction type are fixed value, so the change in the reaction rate constant is due to the difference in the reaction enthalpy. Therefore, with the acid catalyst, the light olefins can be oligomerized to form higher hydrocarbon with higher carbon number. Fig. 4(a) also shows the trend of the rate constants of the cyclization and endo-β scission changing with the carbon number of the reactants. The rate constants of the cyclization reactions are generally larger than those of the endo-β scission, explaining that the yield of aromatics in the product is higher than that of high-carbon olefins. With the increase of the carbon number of the reactant, the rate constant of the cyclization reaction is increased, indicating that the long-chain olefin has a tendency to form a ring structure.

4.3. Influence of the acid strength distribution on the rate constant of various elementary steps

The rate constant of acid strength distribution model is related to the type of reaction. The total acid sites of the zeolite shown in NH_3-TPD can be peak-fitted to five difference spectra with Gaussian distribution, each of which can be identified as a single acid strength site. At the same time, each difference spectrum desorption peak corresponds to the five highest desorption temperatures (about 423, 473, 515, 580, and 620 K), and the DAE corresponding to the five desorption temperatures are 63, 90, 124, 150, and 175 $kJ\cdot mol^{-1}$ respectively. Taking the rate constant at 823 K as an example, and the rate constant at the acid strength site of 63 $kJ\cdot mol^{-1}$ is used as the divisor, the ratio of the rate constant at different acid strength sites was calculated respectively. And the results are shown in Fig. 4(b), it can be seen from Fig. 4(b) that, as revealed by the sensitivity factor, the lower the sensitivity to acid strength, the smaller the growth range of the reaction rate constant with the increase of acid strength. The rate constant of hydride transfer reaction at 175 $kJ\cdot mol^{-1}$ of strong acid site is 1.42 times higher than that at 63 $kJ\cdot mol^{-1}$ of weak acid site. Overall, an increase in catalyst acid strength sites increases the activity of all types of reactions, which has been demonstrated in experiments on acidic zeolites (Nguyen et al., 2011). The rate constants of the methylation/oligomerization reaction, ali-β scission reaction, cyclization reaction and endo-β scission reaction at the strongest acid site reached 2.43, 3.42, 1.98 and 2.37 times compared with those rate constants on the acid sites with DAE = 63 $kJ\cdot mol^{-1}$ respectively. The rate constants of these reactions are largely influenced by the acid strength. This illustrates that appropriately increasing the strong acid sites on the catalyst (DAE = 150 $kJ\cdot mol^{-1}$ and 175 $kJ\cdot mol^{-1}$) will facilitate the aromatization reaction.

4.4. Extend the acid strength distribution kinetic model parameters to propane dehydrogenation with H-ZSM-5

According to the single-event kinetic parameters is not varied with the reactant (Standl et al., 2017), the obtained kinetic parameters were applied for the experimental date of propane dehydroaromatization on H-ZSM-5 in the literature (Bhan et al., 2005) to estimate the kinetic parameters of propane dehydrogenation. In order to verify the kinetic parameter estimation results of the acid strength distribution model, the frequency factor, intrinsic activation energy, and sensitivity factor, etc. obtained by fitting were used as fixed parameters to fit the experimental data of propane dehydroaromatization. The difference elementary steps between propane aromatization and ethylene aromatization are reactions of dehydrogenation of ethane, propane and butane and cracking of propane. The kinetic of propane cracking was fit with the kinetic parameters of ali-β scission elementary steps.

Table 5
Reaction rate of reactions of ethylene aromatization on H-ZSM-5 (Si/Al = 25) in the linear free energy model, the acid strength distribution model and the kinetic model containing subtype elementary steps (Jin et al., 2021) at 823 K and space-time 5.33 $g_{cat}\cdot h\cdot mol^{-1}$.

Reactions	The linear free energy model	The acid strength distribution model	Kinetic model containing subtype elementary steps	Units
$R_1^+ + O_4 \rightarrow R_5^+$	5.50×10^1	7.39×10^2	7.60×10^1 ($r_{alkyl(p:s)}$)	s^{-1} kPa
$R_2^+ + O_3 \rightarrow R_5^+$	8.36×10^3	6.24×10^4	1.12×10^4 ($r_{alkyl(p:s)}$)	s^{-1} kPa
$R_5^+ \rightarrow R_2^+ + O_3$	5.70×10^3	2.69×10^3	1.23×10^3 ($r_{ali\text{-}\beta(s:t)}$)	s^{-1} kPa
$R_5^+ \rightarrow R_{5N}^+$	8.73×10^4	3.50×10^4	4.76×10^4 ($r_{cyclic(s:t)}$)	s^{-1} kPa
$A_6^+ \rightarrow R_6^+$	6.70×10^4	3.87×10^4	1.24×10^4 ($r_{endo\text{-}\beta(s:t)}$)	s^{-1} kPa

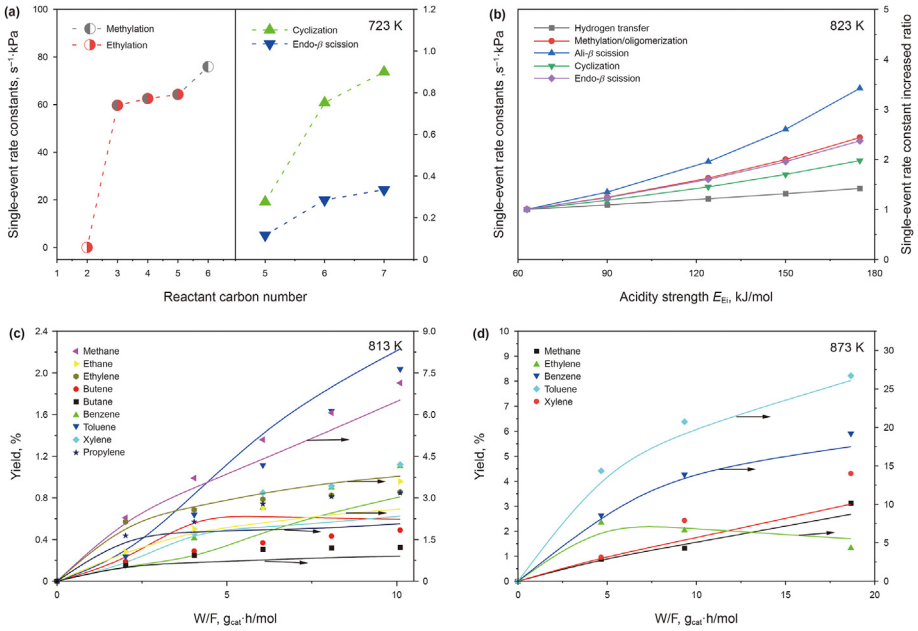

Fig. 4. (**a**) Single-event rate coefficients of the methylation/ethylation, cyclization and endo-β scission of the liner free energy model at 723 K. (**b**) The single event rate coefficients increased ratio with the increase of the acidity strength at 823 K. (**c**) The effect of space time on product yield at different temperature of propane dehydroaromatization with the acid strength distribution model at 813 K in which butane dehydrogenation as a rate control step. (**d**) The effect of space time on product yield at different temperature of ethane dehydroaromatization with the acid strength distribution model at 873 K.

In the literature (Bhan et al., 2005), the value the rate constant of the dehydrogenation reaction and the concentration of propane is relatively higher than other elementary steps and hydrocarbon contents, so the rate of the dehydrogenation reaction is faster than other elementary steps. This suggests that the propane dehydrogenation steps should be treated as thermodynamic equilibrium reaction. Therefore, it was intended to describe the dehydrogenation by the equilibrium constant, and the dehydrogenation reaction is also regarded as an equilibrium reaction in other literatures (Ma and Zou, 2019; Shelepova and Vedyagin, 2020; Van Sint Annaland et al., 2002). At 813 K, the corresponding equilibrium constants in propane dehydroaromatization are shown in Table S14. The fitting result figures shown in Figs. S16, S17 and S18 are residual diagram and parity plot respectively. It can be seen that the model does not fit butane well when the butane equilibrium constant is used. This suggests that butane may not have reached dehydrogenation equilibrium, so butane dehydrogenation will be used as a rate control step in the reaction network. As shown in Fig. 4(c), Figs. S19 and S20, when butane dehydrogenation is used as a rate control step, the fitting results are better than the previous results. It is explained that in the propane dehydroaromatization reaction, ethane and propane dehydrogenation are close to dehydrogenation equilibrium, while butane dehydrogenation is not close to equilibrium, and the rate constant of butane dehydrogenation is shown in Table S15. And this can prove that the kinetic parameters obtained from the acid strength distribution model established for the ethylene aromatization reaction have clear physical meaning and the kinetic parameters in the SEMK model do not change with the feedstock composition.

4.5. Extend the acid strength distribution kinetic model parameters to ethane dehydrogenation with Zn/ZSM-5

In order to further verify the extrapolation of the acid intensity distribution model, the experimental data of ethane dehydroaromatization at 873 K on Zn/ZSM-5 were used for verification. According to the literature (Jin et al., 2018b), the acid strength distribution of Zn/ZSM-5 can be measured by using the desorption activation energy (DAE) of NH_3 as a measure. The acid strength distribution of Zn/ZSM-5 zeolite and the experimental data of ethane dehydroaromatization were substituted into the acid strength distribution model. And use the obtained dynamic parameters such as the frequency factor, intrinsic activation energy, and sensitivity factor as fixed parameters. For the ethane dehydrogenation reaction, use the equilibrium constant of ethane dehydrogenation reaction at 873 K ($K_{C2} = 2.65 \times 10^{-2}$ bar). The fitting results are shown in Fig. 4(d), Figs. S21 and S22, which show that the model fits the experimental data well, indicating that the dehydrogenation of ethane is close to equilibrium. And this further indicates the extrapolation of the SEMK model.

5. Conclusion

In this paper, the SEMK theory combined with linear free energy theory and acid strength distribution concept are used to establish a molecular level kinetic model for ethylene aromatization and ethane dehydroaromatization process on the ZSM-5 catalyst. This extension can reduce the kinetic parameters and simplify the reaction network by comparison with our previous SEMK model including subtype elementary steps based on type of carbenium ions. The rate constants in the linear free energy kinetic model are related with different reaction enthalpy of hydrocarbon and carbenium ion structure. And the rate constant of methylation and oligomerization steps of linear olefins increase with the increase of the chain length of hydrocarbon, so does the rate constant of cyclization of the linear olefin increases in the same way, indicating that the trend for generation aromatics at acid sites. The physisorption and chemisorption heat are separated from the protonation heat in the linear free energy kinetic model, and the obtained physisorption heat and chemisorption heat indicate that carbenium ions with higher carbon numbers can be more stably adsorbed than carbenium with a smaller carbon number.

Moreover, the linear free energy model was extended to the deactivation experimental data of the ethylene oligomerization aromatization reaction on HZSM-5, and the deactivation kinetic parameters were introduced into the model to illustrate the influence of carbon deposition precursors on elementary steps. The established deactivation kinetic model can well fit the trend of experimental data changes with space time. The value of deactivation parameters indicates that the formation of carbon deposition precursor has less impact on two-molecular reactions such as hydrogen transfer and alkylation but has greater impact on cyclization, ali-β scission and endo-β scission and the effect of reducing their reaction rate is more significant.

Furthermore, the concept of acid strength distribution is introduced to the kinetic model to establish the quantitative structure-activity relationship between the acid sites and catalytic performance. By using the NH_3 DPE as a descriptor, the methylation/oligomerization, ali-β scission, cyclization and endo-β scission elementary step were found sensitive to the change of acid strength, which shows that increasing the acid strength of zeolite can promote the aromatization reaction.

The acid strength distribution kinetic model with physisorption heat and chemisorption heat is applied to propane dehydroaromatization reaction network and ethane dehydroaromatization reaction network. It is verified that the parameters of the SEMK model are not affected by the composition of feedstock, indicating that the SEMK model has a good extrapolation. It was confirmed that ethane dehydrogenation was closed to thermodynamic equilibrium in the ethane dehydroaromatization reaction on Zn/ZSM-5. And ethane dehydrogenation and propane dehydrogenation in propane dehydroaromatization on H-ZSM-5 are close to equilibrium, while butane dehydrogenation is not close to equilibrium.

Declaration of interests

The authors declare that they have no known competing financial interests or personal relationships that could have appeared to influence the work reported in this paper.

CRediT authorship contribution statement

Jia-Rong Xie: Investigation, Writing – original draft. **Fang Jin:** Resources, Supervision, Investigation, Conceptualization, Writing.

Acknowledgements

This work was preliminarily supported by the Open Project of Key Laboratory of Green Chemical Engineering Process of Ministry of Education [grant number GCP20190204], Hubei Key Laboratory of Novel Reactor and Green Chemistry Technology (Wuhan Institute of Technology) [grant number 40201005], Engineering Research Center of Phosphorus Resources Development and Utilization of Ministry of Education [grant number LKF201908], and Graduate Innovative Fund of Wuhan Institute of Technology [grant number CX2021028].

Appendix A. Supplementary data

Supplementary data to this article can be found online at https://doi.org/10.1016/j.petsci.2023.07.016.

References

Alwahabi, S.M., Froment, G.F., 2004. Single event kinetic modeling of the methanol–to–olefins process on SAPO–34. Ind. Eng. Chem. Res. 43 (17), 5098–5111. https://doi.org/10.1021/ie040041u.

Baltanas, M.A., Van Raemdonck, K.K., Froment, G.F., et al., 1989. Fundamental kinetic modeling of hydroisomerization and hydrocracking on noble metal–loaded faujasites. 1. Rate parameters for hydroisomerization. Ind. Eng. Chem. Res. 28 (7), 899–910. https://doi.org/10.1021/ie00091a004.

Bhan, A., Hsu, S., Blau, G., et al., 2005. Microkinetic modeling of propane aromatization over HZSM–5. J. Catal. 235 (1), 35–51. https://doi.org/10.1016/j.jcat.2005.07.005.

Borges, P., Ramos Pinto, R., Lemos, M.A.N.D., et al., 2005. Activity–acidity relationship for alkane cracking over zeolites: n–hexane cracking over HZSM–5. J. Mol. Catal. A–Chem. 229 (1), 127–135. https://doi.org/10.1016/j.molcata.2004.11.012.

Brönsted, J.N., 1928. Acid and basic catalysis. Chem. Rev. 5 (3), 231–338. https://doi.org/10.1021/cr60019a001.

Chang, C.D., 1980. A kinetic model for methanol conversion to hydrocarbons. Chem. Eng. Sci. 35 (3), 619–622. https://doi.org/10.1016/0009–2509(80)80011–X.

Chen, N.Y., Reagan, W.J., 1979. Evidence of autocatalysis in methanol to hydrocarbon reactions over zeolite catalysts. J. Catal. 59 (1), 123–129. https://doi.org/10.1016/S0021–9517(79)80050–0.

Clymans, P.J., Froment, G.F., 1984. Computer–generation of reaction paths and rate equations in the thermal cracking of normal and branched paraffins. Comput. Chem. Eng. 8 (2), 137–142. https://doi.org/10.1016/0098–1354(84)87020–9.

Costa, C., Lopes, J.M., Lemos, F., et al., 1999. Activity–acidity relationship in zeolite Y: Part 3. Application of Brönsted type equations. J. Mol. Catal. A–Chem. 144 (1), 233–238. https://doi.org/10.1016/S1381–1169(98)00368–9.

Derouane, E.G., Védrine, J.C., Pinto, R.R., et al., 2013. The acidity of zeolites: concepts, measurements and relation to catalysis: a review on experimental and theoretical methods for the study of zeolite acidity. Catal. Rev. 55 (4), 454–515. https://doi.org/10.1080/01614940.2013.822266.

Froment, G.F., 1991. The modeling of catalyst deactivation by coke formation. Stud. Surf. Sci. Catal. 68, 53–83. https://doi.org/10.1016/S0167–2991(08)62620–8.

Froment, G.F., 1997. Coke formation in catalytic processes: kinetics and catalyst deactivation. Stud. Surf. Sci. Catal. 111, 53–68. https://doi.org/10.1016/S0167–2991(97)80141–3.

Goodarzi, F., Christensen, D.B., Joensen, F., et al., 2020. The effect of active site distribution in bi–functional Pt–zeolite catalysts for ethane dehydroaromatization. Appl. Catal. Gen. 592, 117383. https://doi.org/10.1016/j.apcata.2019.117383.

Hillewaert, L.P., Dierickx, J.L., Froment, G.F., 1988. Computer generation of reaction schemes and rate equations for thermal cracking. AIChE J. 34 (1), 17–24. https://doi.org/10.1002/aic.690340104.

Jin, F., Fan, Y., Yuan, M., et al., 2018a. Single–event kinetic modeling of ethene oligomerization on ZSM–5. Catal. Today 316, 129–141. https://doi.org/10.1016/j.cattod.2018.05.020.

Jin, F., Zhang, P., Wu, G., 2021. Fundamental kinetics model of acidity–activity relation for ethylene oligomerization and aromatization over ZSM–5 zeolites. Chem. Eng. Sci. 229, 116–144. https://doi.org/10.1016/j.ces.2020.116144.

Jin, F., Fan, Y., Wu, G., et al., 2018b. Modified Brønsted type equation with ammonia as probe molecule: quantitative acidity–activity relationship for pyridine synthesis with ZSM–5 catalyst. React. Kinet. Mech. Catal. 123 (2), 517–527. https://doi.org/10.1007/s11144–017–1309–5.

Kumar, H., Froment, G.F., 2007. A generalized mechanistic kinetic model for the hydroisomerization and hydrocracking of long–Chain paraffins. Ind. Eng. Chem. Res. 46 (12), 4075–4090. https://doi.org/10.1021/ie060957w.

Laxmi Narasimhan, C.S., Thybaut, J.W., Marin, G.B., et al., 2003. Kinetic modeling of pore mouth catalysis in the hydroconversion of n-octane on Pt–H–ZSM–22. J. Catal. 220 (2), 399–413. https://doi.org/10.1016/S0021–9517(03)00281–1.

Li, J., Tian, Y., Yan, X., et al., 2020. Approach and potential of replacing oil and natural gas with coal in China. Front. Energy 14 (2), 419–431. https://doi.org/10.1007/s11708–020–0802–0.

Ma, L., Zou, X., 2019. Cooperative catalysis of metal and acid functions in Re–HZSM–5 catalysts for ethane dehydroaromatization. Appl. Catal. B Environ. 243, 703–710. https://doi.org/10.1016/j.apcatb.2018.11.014.

Martinis, J.M., Froment, G.F., 2006. Alkylation on solid acids. Part 2. Single–event kinetic modeling. Ind. Eng. Chem. Res. 45 (3), 954–967. https://doi.org/10.1021/ie050910v.

Mihail, R., Straja, S., Maria, G., et al., 1983. A kinetic model for methanol conversion to hydrocarbons. Chem. Eng. Sci. 38 (9), 1581–1591. https://doi.org/10.1016/0009–2509(83)80094–3.

Moustafa, T.M., Froment, G.F., 2003. Kinetic modeling of coke formation and deactivation in the catalytic cracking of vacuum gas oil. Ind. Eng. Chem. Res. 42 (1), 14–25. https://doi.org/10.1021/ie0204538.

Nawaz, Z., 2015. Light alkane dehydrogenation to light olefin technologies: a comprehensive review. Rev. Chem. Eng. 31 (5), 413–436. https://doi.org/10.1515/revce–2015–0012.

Nguyen, C.M., De Moor, B.A., Reyniers, M., et al., 2011. Physisorption and chemisorption of linear alkenes in zeolites: a combined QM–Pot(MP2//B3LYP:GULP)–statistical thermodynamics study. J. Phys. Chem. C 115 (48), 23831–23847. https://doi.org/10.1021/jp2067606.

Nguyen, C.M., De Moor, B.A., Reyniers, M., et al., 2012. Isobutene protonation in H–FAU, H–MOR, H–ZSM–5, and H–ZSM–22. J. Phys. Chem. C 116 (34), 18236–18249. https://doi.org/10.1021/jp304081k.

Park, T., Froment, G.F., 2001a. Kinetic modeling of the methanol to olefins process. 1. Model formulation. Ind. Eng. Chem. Res. 40 (20), 4172–4186. https://doi.org/10.1021/ie0008530.

Park, T., Froment, G.F., 2001b. Kinetic modeling of the methanol to olefins process.

2. Experimental results, model discrimination, and parameter estimation. Ind. Eng. Chem. Res. 40 (20), 4187–4196. https://doi.org/10.1021/ie000854s.
Park, T., Froment, G.F., 2004. Analysis of fundamental reaction rates in the methanol–to–olefins process on ZSM–5 as a basis for reactor design and operation. Ind. Eng. Chem. Res. 43 (3), 682–689. https://doi.org/10.1021/ie030130r.
Pirro, L., Mendes, P.S.F., Paret, S., et al., 2019. Descriptor–property relationships in heterogeneous catalysis: exploiting synergies between statistics and fundamental kinetic modelling. Catal. Sci. Technol. 9, 3109–3125. https://doi.org/10.1039/C9CY00719A.
Robinson, B., Bai, X., Samanta, A., et al., 2018. Stability of Fe–and Zn–promoted Mo/ZSM–5 catalysts for ethane dehydroaromatization in cyclic operation mode. Energy Fuel. 32 (7), 7810–7819. https://doi.org/10.1021/acs.energyfuels.8b01516.
Schoenfelder, H., Hinderer, J., Werther, J., et al., 1994. Methanol to olefins—prediction of the performance of a circulating fluidized–bed reactor on the basis of kinetic experiments in a fixed–bed reactor. Chem. Eng. Sci. 49 (24, Part 2), 5377–5390. https://doi.org/10.1016/0009–2509(94)00332–7.
Shelepova, E.V., Vedyagin, A.A., 2020. Intensification of the dehydrogenation process of different hydrocarbons in a catalytic membrane reactor. Chem. Eng. Process 155, 108072. https://doi.org/10.1016/j.cep.2020.108072.
Standl, S., Kirchberger, F.M., Kühlewind, T., et al., 2020. Single–event kinetic model for methanol–to–olefins (MTO) over ZSM–5: fundamental kinetics for the olefin co–feed reactivity. Chem. Eng. J. 402, 126023. https://doi.org/10.1016/j.cej.2020.126023.
Standl, S., Tonigold, M., Hinrichsen, O., 2017. Single-event kinetic modeling of olefin cracking on ZSM–5: proof of feed independence. Ind. Eng. Chem. Res. 56 (45), 13096–13108. https://doi.org/10.1021/acs.iecr.7b01344.
Toch, K., Thybaut, J.W., Marin, G.B., 2015. Ethene oligomerization on Ni–SiO_2–Al_2O_3: experimental investigation and Single–Event MicroKinetic modeling. Appl. Catal. Gen. 489, 292–304. https://doi.org/10.1016/j.apcata.2014.10.036.
Van Sint Annaland, M., Scholts, H.A.R., Kuipers, J.A.M., et al., 2002. A novel reverse flow reactor coupling endothermic and exothermic reactions: Part II: sequential reactor configuration for reversible endothermic reactions. Chem. Eng. Sci. 57 (5), 855–872. https://doi.org/10.1016/S0009–2509(01)00423–7V.
Vojtko, J., Tomčík, P., 2014. A Method for Esterification Reaction rate prediction of aliphatic monocarboxylic acids with primary alcohols in 1,4–dioxane based on two parametrical taft equation. Int. J. Chem. Kinet. 46 (3), 189–196. https://doi.org/10.1002/kin.20845.
Vynckier, E., Froment, G.F., 1991. Modeling of the kinetics of complex processes based upon elementary steps. In: Gianni, A., Stanley I, S. (Eds.), Kinetic and Thermodynamic Lumping of Multicomponent Mixtures. Elsevier, Amsterdam, pp. 131–161. https://doi.org/10.1016/B978–0–444–89032–0.50011–6.
Wang, C., Wang, L., Wu, G., et al., 2020. Quantitative relationship between activity and acid site distribution in the oligomerization of ethylene over MCM–41 catalyst. Catal. Lett. 150 (2), 429–437. https://doi.org/10.1007/s10562–019–02938–w.
Wang, Y., Cipolletta, M., Vernières-Hassimi, L., et al., 2019. Application of the concept of linear free energy relationships to the hydrogenation of levulinic acid and its corresponding esters. Chem. Eng. J. 374, 822–831. https://doi.org/10.1016/j.cej.2019.05.218.
Xu, B., Tan, M., Wu, X., et al., 2021. Effects of silylation on Ga/HZSM–5 for improved propane dehydroaromatization. Fuel 283, 118889. https://doi.org/10.1016/j.fuel.2020.118889.
Zhang, Y., Yao, W., Fang, H., et al., 2015. Catalytic alkane dehydrogenations. Sci. Bull. 60 (15), 1316–1331. https://doi.org/10.1007/s11434–015–0818–8.
Zhou, L., Froment, G.F., Yang, Y., et al., 2016. Advanced fundamental modeling of the kinetics of Fischer–Tropsch synthesis. AIChE J. 62 (5), 1668–1682. https://doi:10.1002/aic.15141.